

Analysis of a Cuspidal 6R Robot

Alexander Feeß and Martin Weiß

OTH Regensburg, 93053 Regensburg, Germany,
alexander.feess@oth-regensburg.de
martin.weiss@oth-regensburg.de

Abstract. We present a theoretical and numerical analysis of the kinematics for the *Transpressor*, a cuspidal 6R robot. It admits up to 16 inverse kinematics solutions which are described geometrically. For special target poses, we provide the solutions analytically, and present a simple numerical solver for the general case. Moreover, an estimation of the Jacobian determinant on a path between two solutions proves cuspidality for a class of robots similar to the transpressor.

To the best of the authors' knowledge this is the first 6R robot where singularity free paths are provided for a wide class of solutions, without the need for numerical investigations.

Keywords: Cuspidal robots, Singularity free paths, Inverse kinematics

1 Introduction

A general 6R robot may have up to 16 inverse kinematic solutions (IKS), ignoring joint limits. This was proven in [8] and a first numerical example showing that the bound is sharp is given in [7]. Most commercial robots have their last 3 axes intersecting (spherical wrist) and a simple regional structure, resulting in 8 solutions. With the recent rise in popularity of cobots, new manipulators with differing structures appeared, including models with non-spherical wrists. These can have advantages in their construction, but are mathematically more challenging, as discussed in [10, 4]. For some of these, the inverse kinematics problem can be solved analytically and might even still have only 8 solutions like the Universal Robot URx series [5, 13]. But generally, there are up to 16 solutions, and no analytical solution is known e.g. for the FANUC CRX-10ia/L, Yaskawa HC10DTP and Kinova Link 6.

One property that is expected of these models is *cuspidality*: A non-singular motion from one IKS to another is possible. This effect has mostly been studied for 3R robots, where a characterization of this property has been established and classification results exist, see [12]. For 6R manipulators, these are still open problems. Numerical investigations of specific robots include [3, 10, 1], an open conjecture on the cuspidality is stated in [9].

We analyze a 6R kinematic inspired by the KUKA Transpressor [6]. This robot is derived from a standard KUKA KR100P, but has axis 6 shifted away in parallel from the wrist center as shown in Fig. 1. This makes the wrist non-spherical, and no analytical inverse kinematic solution is known. Our simplified

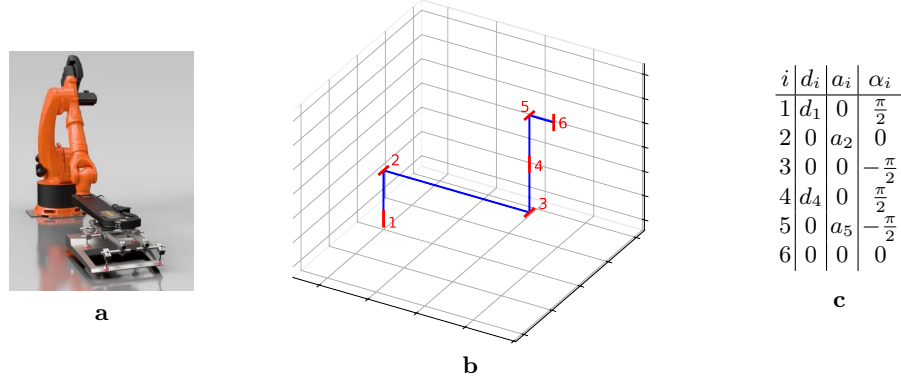


Fig. 1. **a** The KUKA Transpressor, **b** our simplified version in home position (the red indication of axis 4 is shifted along z_4 for visibility), and **c** the table of DH-parameters

version has intersections of axes 1 and 2, as well as axes 3 and 4, whereas the original robot has offsets between these axes. We investigate the IKS of this model and show its cuspidality.

We proceed as follows: After introducing notation and describing the robot kinematics in Sect. 2, we extend the work of [11] in Sect. 3 by providing a numerical approach for the general IKS and introducing another class of end effector poses with analytical solutions. This allows us to show the existence of a singularity-free change of IKS by analytical means in Sect. 4.

2 Robot Model

For any $T \in \text{SE}(3)$ we denote the rotational part by R and the translation by p . The world coordinate system is set to align with the first axis $T_1 = T_{\text{world}}$. For DH-parameters a_i, d_i and α_i , we have

$$T_{i+1} = T_i \cdot \text{Rot}_z(\theta_i) \cdot \text{Transl}_z(d_i) \cdot \text{Transl}_x(a_i) \cdot \text{Rot}_x(\alpha_i) .$$

The end effector or target pose is denoted by T_E and since we consider a 6R manipulator, we have $T_E = T_7$ with the convention above. The coordinate axes of T_i are denoted by x_i, y_i and z_i , when referring to the world coordinate system we might omit the subscript.

Fig. 1c shows the DH-parameters of the class of robots considered. For computations, we always set $d_1 = 0$, as different values can simply be compensated by moving the origin along the z -axis. Only in the visualizations we have $d_1 = 1$ and for the indication of joint axes we depicted axis 4 shifted along z_4 to make the distinction between the axes easier (while actually the translational parts of T_3 and T_4 coincide). For visualizations and examples we usually set $a_2 = 3$, $d_4 = 2$ and $a_5 = 1/2$. The analytical and numerical methods for computing the inverse kinematic solutions described in Sect. 3 can be applied for any choice of the non-zero parameters.

3 Inverse Kinematic Solutions

After revisiting the kinematic of the regional 3R chain composed of the initial three axes, we present a numerical approach to solve the inverse kinematic of the transpressor in general. We provide analytical solutions for poses with vertical z_E -axis, as well as for poses on the z_1 -axis with a special orientation R_E . In both cases up to 16 solutions exist. For the latter class we will provide a singularity free change of solutions in Sect. 4.

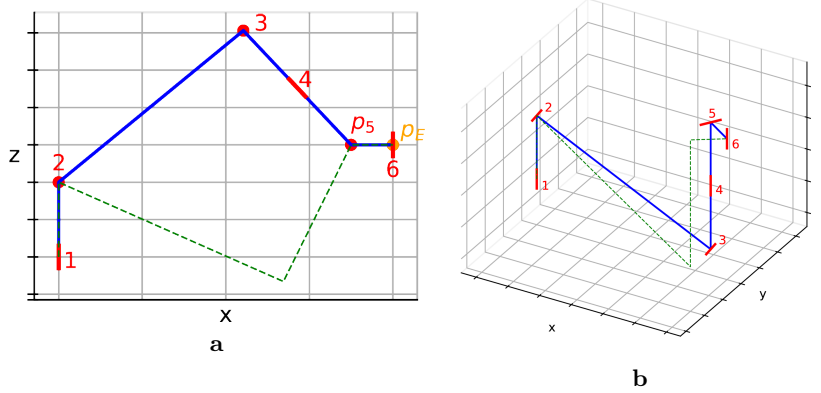


Fig. 2. Some IKS for a pose with vertical z_E -axis with **a** elbow up/down configurations, wrist outwards, and **b** left/right configurations, elbow down

3.1 Kinematic of the Initial 3R-Chain

We consider the 3R regional manipulator obtained by restricting to the first three joints of the robot with target position p_5 , the fifth joint. The angle θ_4 can be ignored or fixed, as it only affects the orientation of T_5 . To compute the inverse kinematic with target $p_5 = (p_{5,x}, p_{5,y}, p_{5,z})$ we set $\theta_1 = \arctan(p_{5,y}/p_{5,x})$ and then are able solve a planar 2R chain for the other joints. This is illustrated in Fig. 2a and yields two solutions, commonly characterized as *elbow up* or *down*. Rotating θ_1 by π yields another two solutions. Explicitly, for any solution $(\theta_1, \theta_2, \theta_3)$ we can reach the same position with $(\theta_1 + \pi, -\theta_2 + \pi, -\theta_3 + \pi)$. This is called a *shoulder flip*. In the reachable workspace, this 3R-chain has generally exactly these four solutions, the only exception being singular configurations.

Remark 1. The shoulder flip can be generalized to the entire chain, one only has to correct the orientation of T_5 by rotating θ_4 half a turn, i.e., the joint values $(\theta_1 + \pi, -\theta_2 + \pi, -\theta_3 + \pi, \theta_4 + \pi, \theta_5, \theta_6)$ yield the same pose as $(\theta_1, \theta_2, \theta_3, \theta_4, \theta_5, \theta_6)$.

This does not work for the elbow change, as for $\theta_4 \neq 0, \pi$ we are generally not able achieve the same orientation at axis 5 in both configurations.

3.2 General Approach

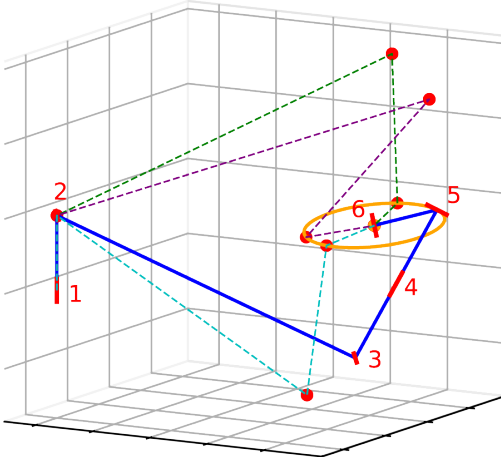


Fig. 3. A pose with 4 IKS, 2 in each elbow configuration. Considering both shoulder configurations yields a total of 8 IKS. For the solid blue configuration, we indicated the direction of the axes with red lines. Note that axis 5 is tangential to the circle.

Let T_E be a target pose and A the x_Ey_E -plane. The last link has length a_5 , therefore p_5 has to lie on a circle S on A with center p_E and radius a_5 (depicted in orange in Fig. 3). Additionally, we need the axis z_5 to be tangential to S . Since axes 4 and 5 are orthogonal and intersect each other, we can equivalently ask for z_4 to be orthogonal to the tangent $t(p_5)$ to S at p_5 . As noted in Sect. 3.1, p_5 only depends on the first three axes. Therefore, the inverse kinematics problem can be reduced to regarding the initial 3R-chain and investigating when it can reach $p_5 \in S$ with $z_4 \perp t(p_5)$. By Remark 1 if one such solution is found, a second solution always exists via a shoulder flip, but the other elbow configuration has to be inspected separately.

This can be computed numerically, by discretizing the circle S , computing one IKS of the 3R-chain on each point, and evaluating the inner product of z_4 and $t(p_5)$. While increasing the number of sample points results in higher accuracy, the number of solutions is usually already correct with $n = 50$, as this is only critical when distinct IKS only differ marginally (e.g. near a singularity).

3.3 Poses with Vertical z_E -Axis

In this section we provide an analytical method to compute all IKS for target poses with $z_E \parallel z_1$. For simplicity, we may even assume T_E to be a pure translation, as we can always achieve this by an appropriate choice of θ_6 . Similarly, we can restrict to poses on the xz -half-plane with positive x -values, and get the other positions by rotating about θ_1 .

The fundamental observation for these considerations is the following: The plane A described in Sect. 3.2 is now parallel to the x_1y_1 -plane. For any configuration $(\theta_1, \theta_2, \theta_3)$ with $p_5 \in A$, the rotation of joint 4 can be regarded as a circle around p_5 , which the z_5 -unit vector traces. This circle intersects A exactly twice, at the values $\theta_4 = 0$ and $\theta_4 = \pi$. This means these poses can generally only be reached if all links align (projected along the z -axis). For fixed elbow and shoulder configuration of the 3R-chain, this yields up to two solutions with the wrist either facing *out*- or *inwards*. In total, this results in up to 8 IKS, for which the remaining joint values are computed by solving the 3R inverse kinematics for $p_5 = (p_{E,x} \pm a_5, 0, p_{E,z})$. The wrist out configuration is shown in Fig. 2a.

There exists an additional possibility to reach these poses if there is a point on S that can be achieved with $z_4 \parallel z_1$. Then the z_5 -axis lies in A for any θ_4 and we can choose a suitable value to get $z_4 \perp t(p_5)$. If we can reach a target pose that way with θ_4 as the fourth joint value, we can also reach it from a similar pose with $\theta'_4 = -\theta_4$. Therefore, these solutions always appear in pairs of a *left* and *right* configuration as depicted in Fig. 2b. In this case we have to be more careful about the configuration of the 3R-chain, as usually changing the elbow configuration changes the direction of z_4 . Thus we need to separately check both possibilities and it might be that in neither, both or only in one elbow configuration the special solutions can be obtained.

Explicitly, consider a target pose as above, with orientation identical to the orientation of T_1 , and translational part $p_E = (p_{E,x}, 0, p_{E,z})$ with $p_{E,x} \geq 0$. The condition $z_4 \parallel z_1$ is satisfied if and only if $\theta_3 = \pi - \theta_2$ in the elbow up configuration and $\theta_3 = -\theta_2$ with elbow down. If $p_{5,z} = p_{E,z}$ can be achieved, then there exists exactly one pair (θ_2, θ_3) for each shoulder configuration. Fixing these, we consider the distance ρ_5 with $\rho_5^2 = p_{5,x}^2 + p_{5,y}^2$. Now we can find a solution if and only if $|\rho_5 - \rho_E| \leq a_5$. In the case of equality, both solutions coincide with one of the solutions with wrist out- or inwards. Given a strict inequality, we obtain exactly two solutions, and readily compute the remaining angles to approach p_E from two sides. Considering both elbow and shoulder configurations, we obtain up to 8 additional solutions. Analytic formulas are possible.

3.4 Poses on z_1 -Axis

For the subsequent analysis, we recall the second family of poses with analytical inverse kinematics solutions. For a more detailed description we refer to [11]. The results can be applied to target poses of the form

$$T_E = \begin{pmatrix} 0 & 0 & 1 & 0 \\ 0 & 1 & 0 & 0 \\ -1 & 0 & 0 & p_{E,z} \\ 0 & 0 & 0 & 1 \end{pmatrix}. \quad (1)$$

With these, we can obtain solutions either by aligning the wrist extension with the z_1 -axis (*left/right configurations*) or with the z_4 -axis (*back/front configurations*). Switching between left and right (or back and front) is achieved by a

shoulder flip. Each of these again has two possible directions of the wrist (*flipped or not*). Finally, all of these can be reached in both elbow configurations, yielding up to 16 solutions. Two of the four configurations are shown in Fig. 4. Formulas are given in [11].

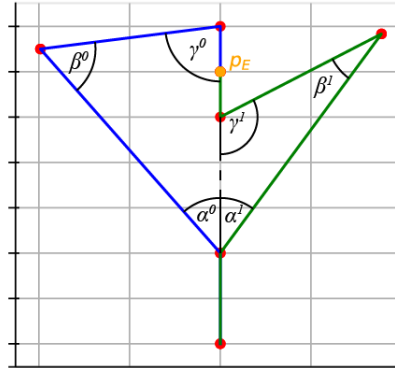


Fig. 4. Two configurations to reach a pose on the z -axis: left configuration with elbow up and no wrist flip (blue), and right configuration with elbow up and wrist flipped (green)

3.5 Number of IKS

For both analytical approaches, the number of IKS can be 0, 4, 8, 12 or 16, depending on the target pose. Applying the numerical algorithm indicates that the same holds generally, but grouping these solutions remains an open challenge.

4 Singularity-free Change of Solution

We now provide a singularity-free motion between two solutions $\theta^0, \theta^1 \in \mathbb{R}^6$, reaching the same end effector pose. We regard the configurations depicted in Fig. 4, the joint values are provided in Table 1.

As an example we prove that the linear path $\theta(\lambda) = \theta^0 + \lambda(\theta^1 - \theta^0)$, $\lambda \in [0, 1]$ is without singularity for a wide range of parameters.

Table 1. The two configurations investigated

	θ_1	θ_2	θ_3	θ_4	θ_5	θ_6	description
θ^0	0	$\frac{\pi}{2} - \alpha^0$	$\frac{\pi}{2} - \beta^0$	0	$-\frac{\pi}{2} - \gamma^0$	0	shoulder left, elbow up, no wrist flip
θ^1	π	$\frac{\pi}{2} - \alpha^1$	$\frac{\pi}{2} - \beta^1$	0	$\frac{\pi}{2} - \gamma^1$	π	shoulder right, elbow up, wrist flipped

The determinant of the Jacobian is

$$-a_2c_3(((s_3d_4^2 - a_2d_4)s_5 + a_5(a_2c_4^2 + d_4s_3 - a_2))c_2 + s_2d_4c_3(s_5d_4 + a_5)) . \quad (2)$$

We abbreviate $s_i = \sin(\theta_i)$ and $c_i = \cos(\theta_i)$. The value $\theta_4(\lambda) = 0$ is constant and therefore $c_4 = 1$, simplifying (2) to

$$\begin{aligned} & -a_2c_3(((s_3d_4^2 - a_2d_4)s_5 + a_5d_4s_3))c_2 + s_2d_4c_3(s_5d_4 + a_5) \\ & = -a_2d_4c_3((s_3d_4 - a_2)s_5 + a_5 \sin(\theta_2 + \theta_3) + s_2c_3s_5d_4) \\ & = -a_2d_4c_3(((s_3 + s_2c_3)d_4 - a_2)s_5 + a_5 \sin(\theta_2 + \theta_3)) \end{aligned} \quad (3)$$

The factor c_3 in front of the bracket does not change its sign if $0 < \beta^k < \pi/2$ for $k = 0, 1$. A sufficient condition is that the triangle $\Delta(d_4, z + a_5, a_2)$ for configuration θ^0 has an acute angle β^0 , then also $\Delta(d_4, z - a_5, a_2)$ for configuration θ^1 has an acute angle β^1 for monotonicity reasons. To achieve this, $|p_{E,z} \pm a_5|$ must be small compared to a_2 and d_4 .

The bracket contains a summand with factor $\sin(\theta_2 + \theta_3)$ and one with factor $\sin(\theta_5)$. We give sufficient conditions for both summands to be positive.

We have $\alpha^k + \beta^k + \gamma^k = \pi$ for both $k = 0, 1$. From Table 1 we see that $\theta_2 + \theta_3 = \pi - \alpha^k - \beta^k = \gamma^k$ for both poses 0 and 1. Moreover, $\theta_5^0 = -\pi/2 - \gamma^0$ and $\theta_5^1 = \pi/2 - \gamma^1$. In both cases $\sin(\theta_5) = \pm \cos(\theta_2 + \theta_3)$, so one of the sin values will be close to 0 if the other is close to 1 in absolute value.

Choosing γ close to $\pi/2$, we see that $\sin(\theta_2(\lambda) + \theta_3(\lambda))$ has positive values near 1 in the interval between γ^0 and γ^1 because $\theta_2(\lambda) + \theta_3(\lambda) = \gamma^0 + \lambda(\gamma^1 - \gamma^0)$ holds on the whole connection.

This suggests choosing $p_{z,E}$ such that the triangle $\Delta(d_4, p_{E,z}, a_2)$ with sides $p_{z,E}$, a_2 and d_4 has a right angle at p_E . With this choice, we observe in Fig. 4 that $0 < \gamma^0 < \pi/2$ and $\pi/2 < \gamma^1 < \pi$. This translates into $-\pi < \theta_5^0 < 0$ and $-\pi/2 < \theta_5^1 < 0$. So we have $\sin(\theta_5(\lambda)) < 0$ for all $\lambda \in [0, 1]$. The term before $\sin(\theta_5)$ can be made negative if we require $a_2 > 2d_4$. We conclude that the bracket term in (3) is positive.

Numerical computations show that the estimates are quite conservative. Our usual example values $a_2 = 3, d_4 = 2, a_5 = 1/2$ violate the condition $\sin(\theta_5(\lambda)) < 0$ slightly at the boundaries of the interval but the determinant still does not change sign.

The above provides an analytical way of showing cuspidality for a range of different DH-parameters. Generalizing this to other solution pairs and different DH-parameters can get cumbersome. For the parameter values $a_2 = 3, d_4 = 2$ and $a_5 = 1/2$ we investigated these solution changes also numerically. Considering again the solutions of Sect. 3.4, one can group the 16 IKS into 4 classes of 4 solutions such that within each class, the sign of each of the two factors in the Jacobi Determinant does not change. While there exist more elaborate approaches to detect connectedness [2], we discovered that just a small adjustment to a linear motion (e.g. by translating the path slightly along θ_1) leads to a singularity-free path between any two solutions in the same class. This means all IKS of one class are in the same aspect, i.e., a singularity-free region in joint space.

5 Conclusion and Outlook

We provided algorithms to compute the IKS of a class of robots with up to 16 solutions. Moreover, the cuspidality property for a range of parameters was established and proved analytically.

The results suggest that further investigation might prove fruitful, but even this simple architecture shows that the analysis of 6R cuspidal robots is challenging: An analytical solution for the entire workspace would be desirable, but the results of Sects. 3.3 and 3.4 do not easily generalize.

It would be useful to classify the configurations into singularity-free groups by their parameter values and establishing partitions of work- and joint space where movement avoiding singular configurations is possible. There, studying the singular variety and symmetries in the IKS could be helpful. Understanding these kinematic properties is essential to safe and efficient motion planning.

References

1. Abbes, M., Poisson, G.: Geometric Approach for Inverse Kinematics of the FANUC CRX Collaborative Robot, *Robotics* 13(6), pp. 91–103 (2024)
2. Capco, J., Din, M.S.E., Schicho, J.: Robots, computer algebra and eight connected components. In: Proceedings of the 45th International Symposium on Symbolic and Algebraic Computation, pp. 62–69 (2020).
3. Carbonari, L., Palpacelli, M., Callegari, M.: Inverse Kinematics of a Class of 6R Collaborative Robots with Non-Spherical Wrist, *Robotics* 12(2), pp. 36–53 (2023)
4. Elias, A.J., Wen, J.T.: Path Planning and Optimization for Cuspidal 6R Manipulators, <http://arxiv.org/pdf/2501.18505v1> (2025)
5. Keating, R.: UR5 Inverse Kinematics. Johns Hopkins University (2014)
6. KUKA AG: Revolutionizing Press Automation: The Comprehensive KUKA.PressAutomation Solution <https://marketscale.com/shows/kuka/> (2023)
7. Manseur, R., Doty, K.L.: A Robot Manipulator With 16 Real Inverse Kinematic Solution Sets. *The International Journal of Robotics Research* 8(5), pp. 75–79 (1989)
8. Primrose, E.J.F.: On the input-output equation of the general 7R-mechanism. *Mechanism and Machine Theory* 21(6), pp. 509–510 (1986)
9. Salunkhe, D.H.: Cuspidal robots : theoretical study, classification, and application to commercial robots. Ph.D. thesis, École centrale de Nantes (2023)
10. Salunkhe, D.H., Chablat, D., Wenger, Ph.: Trajectory planning issues in cuspidal commercial robots. *IEEE International Conference on Robotics & Automation*, pp. 7426–7432 (2023)
11. Weiß, M.G.: A Class of 6R Robots and Poses with 16 Analytical Solutions, *Proceedings of the IMA Conference on Mathematics of Robotics* (2015)
12. Wenger, Ph.: Cuspidal Robots. In: Springer (ed.) *Singular Configurations of Mechanisms and Manipulators*, pp. 67–99 (2019)
13. Yang, T., Tian, Y., Wang, Q., Wang, Y., Jiang, L., Li, G.: Kinematics Analysis and Trajectory Planning of UR5 Robot, *2023 2nd International Conference on Automation, Robotics and Computer Engineering (ICARCE)*, pp. 1–4 (2023)